

Rapid Accurate Calculation of the s -wave Scattering Length

Vladimir V. Meshkov and Andrey V. Stolyarov*

Department of Chemistry, Moscow State University, Moscow, 119991, Russia

Robert J. Le Roy

*Guelph-Waterloo Center for Graduate Work in Chemistry and Biochemistry,
University of Waterloo, Waterloo, Ontario N2L 3G1, Canada*

(Dated: February 18, 2022)

Transformation of the conventional radial Schrödinger equation defined on the interval $r \in [0, \infty)$ into an equivalent form defined on the finite domain $y(r) \in [a, b]$ allows the s -wave scattering length a_s to be exactly expressed in terms of a logarithmic derivative of the transformed wave function $\phi(y)$ at the outer boundary point $y = b$, which corresponds to $r = \infty$. In particular, for an arbitrary interaction potential that dies off as fast as $1/r^n$ for $n \geq 4$, the modified wave function $\phi(y)$ obtained by using the two-parameter mapping function $r(y; \bar{r}, \beta) = \bar{r} \left[1 + \frac{1}{\beta} \tan(\pi y/2) \right]$ has no singularities, and

$$a_s = \bar{r} \left[1 + \frac{2}{\pi\beta} \frac{1}{\phi(1)} \frac{d\phi(1)}{dy} \right].$$

For a well bound potential with equilibrium distance r_e , the optimal mapping parameters are $\bar{r} \approx r_e$ and $\beta \approx \frac{n}{2} - 1$. An outward integration procedure based on Johnson's log-derivative algorithm [B.R. Johnson, *J. Comp. Phys.*, **13**, 445 (1973)] combined with a Richardson extrapolation procedure is shown to readily yield high precision a_s -values both for model Lennard-Jones ($2n, n$) potentials and for realistic published potentials for the Xe-e⁻, Cs₂($a^3\Sigma_u^+$) and ^{3,4}He₂($X^1\Sigma_g^+$) systems. Use of this same transformed Schrödinger equation was previously shown [V.V. Meshkov *et al.* *Phys. Rev. A*, **78**, 052510 (2008)] to ensure the efficient calculation of all bound levels supported by a potential, including those lying extremely close to dissociation.

PACS numbers: 31.15.-p; 34.50.-s; 37.10.De

I. INTRODUCTION

The so-called the s -wave scattering length a_s is a key parameter for describing the interaction of particles at very low collision energies. In particular, the two-body collision problem is completely specified by the scattering length in the low temperature limit where the elastic cross section becomes $\sigma_e = 4\pi a_s^2$ [1, 2]. Many of the properties of a Bose-Einstein condensate [3] also depend only on the scattering length. In particular, the chemical potential of a uniform Bose gas is simply proportional to the a_s -value [4], namely: $\mu_{Bose} = a_s n 4\pi \hbar^2 / m$, where n is the number density and m is the atomic mass [5]. Thus, positive a_s values correspond to overall repulsive interactions while negative values correspond to attractive ones.

The scattering length is asymptotically related to the scattering phase shift $\eta_s(k)$ by the expression [1, 2, 6]:

$$a_s = - \lim_{k \rightarrow 0} \frac{\tan \eta_s(k)}{k} \quad (1)$$

in which k is the relative wave vector of the colliding particles. The scattering length can be also determined from

the wavefunction $\psi(r)$ of the radial Schrödinger equation

$$- \frac{d^2 \psi(r)}{dr^2} = Q(r) \psi(r) \quad (2)$$
$$Q(r) \equiv - \frac{2\mu}{\hbar^2} U(r)$$

solved at zero energy $E = 0$ with the inner boundary condition $\psi(0) = 0$. It has been proved [1] that for arbitrary potentials $U(r)$ that obey the asymptotic condition:

$$\lim_{r \rightarrow \infty} r^n U(r) = 0 \quad \text{for } n > 3, \quad (3)$$

the wavefunction $\psi(r)$ has the linear asymptotic form

$$\psi(r) \simeq S(r - a_s), \quad r \rightarrow \infty, \quad (4)$$

in which the slope S is a constant. It can be seen from Eq.(4) that the scattering length physically corresponds to the distance where the continuation of this asymptotic straight line crosses the r -axis. It is clear that the value of a_s will be strongly depend on the interaction potential $U(r)$ and on the reduced mass of the colliding particles μ . It is also well known that the scattering length a_s is approximately related to the binding energy $E_{v_{\max}}^b \geq 0$ of the highest bound level ($v = v_{\max}$) of the interaction potential $U(r)$ [7]:

$$a_s \approx \sqrt{\frac{\hbar^2}{2\mu E_{v_{\max}}^b}} \quad (5)$$

* Email me at: avstol@phys.chem.msu.ru

It is clear that $a_s \rightarrow +\infty$ as $E_{v_{\max}}^b \rightarrow 0$, while a_s will take on large negative values if the potential well is almost deep enough to support one more bound level. In other words, depending on the potential and the reduced mass, the scattering length can have any value on the interval $(-\infty, +\infty)$.

Accurate determination of scattering lengths determined from photoassociation of ultracold colliding atoms [8] offers the possibility of constructing reliable empirical interatomic potentials all the way to the dissociation limit [9, 10]. However, rapid and robust methods for performing scattering length calculations are required to make such an inversion procedure feasible. Furthermore, a high degree of accuracy in the calculated a_s -values is required in order to provide the accurate derivatives of the scattering length with respect to the parameters defining the potential that are required for performing such fits [11].

There are a number of existing schemes for calculating scattering lengths. However, calculation of the scattering phase shift $\eta_s(k)$ as a function of energy [1, 2] in order to apply the low-energy extrapolation of Eq. (1) leads to large uncertainties, especially for large a_s values, since $\eta_s(k)$ becomes a very steep function in the vicinity of $k = 0$. Moreover, the direct numerical integration of the radial equation (2) cannot be performed easily because the asymptotic linear form of Eq. (4) is only reached at very large distances r , typically thousands of Å. More robust methods [11–13] are based on integration of Eq. (2) to some finite matching distance r_m , and then matching the resulting numerical wave function $\psi(r_m)$ with an asymptotic counterpart for the long-range region which is known analytically for particular kinds of potentials. Alternatively, the influence of a long-range interaction on the truncated apparent a_s -value at some distance $r = r_m$ can be effectively corrected in the framework of a secular perturbation theory expansion [14]. These asymptotic methods often yield fairly accurate results, but not for large a_s values. Moreover, they all require additional computational effort to ensure the convergence of results with respect to an optimal r_m value whose position is not well-defined *a priori*. These asymptotic methods also cannot readily be used for potentials for which the asymptotic solution is not available in closed form. We also note that a very elegant analytical formula for a_s has been obtained using the semiclassical approximation for the wavefunction $\psi(r)$ [15]. However, while that formula can be useful for estimation purposes, its accuracy is limited by its dependence on the WKB approximation [1, 16], so it does not suffice for many applications.

The key to the present method is the analytically exact transformation [17, 18] of the initial Schrödinger equation (2) defined on infinite domain $r \in [0, \infty)$ into a modified radial equation defined by a reduced variable $y(r)$ on a finite interval $y(r) \in [a, b]$ [19, 20]. The resulting transformed equation can be solved very efficiently by standard numerical methods [21, 22]. Moreover, we show that a special choice of the mapping function $r(y)$

leads to a transformed wave function $\phi(b)$ that has no singularities on the interval $[a, b]$. In this case the scattering length can be expressed analytically in terms of the logarithmic derivative of the solution at the (finite) end point b and the associated mapping parameters. One efficient way to obtain the required logarithmic derivatives of the wave function at $y = b$ is to numerically integrate the resulting modified Riccati equation using Johnson's log-derivative method [23, 24] and apply a Richardson extrapolation to the values obtained at the limit [25, 26]. A FORTRAN code applying this approach that has been applied both to model Lennard-Jones $(2n, n)$ potentials and to realistic potentials for $\text{Cs}_2(a^3\Sigma_u^+)$ [12, 13, 15], Xe-e^- [27] and $^3,4\text{He}_2(X^1\Sigma_g^+)$ [28] taken from the literature has been provided as Supplementary Documentation [29]. An alternate version of the present approach based on the conventional Numerov propagator [21] has been implemented in a 'finite domain' version of the general purpose bound-state/Franck-Condon code LEVEL [30].

II. ADAPTIVE MAPPING PROCEDURE FOR SCATTERING LENGTH CALCULATIONS

A. Reduced variable transformation of the radial equation

We begin by introducing a mapping function $y = y(r)$ that is a smooth, monotonically increasing function of the radial coordinate r and maps $[0, \infty)$ onto the finite domain $[a, b]$. The well-known substitution [17, 18]

$$\psi(r(y)) = \sqrt{g(y)} \phi(y) \quad , \quad g(y) \equiv \frac{dr}{dy} > 0 \quad (6)$$

then transforms the conventional radial Schrödinger equation (2) into the equivalent form

$$\frac{d^2\phi(y)}{dy^2} = -\tilde{Q}(y) \phi(y) \quad (7)$$

in which

$$\tilde{Q}(y) \equiv g^2(y) Q(r(y)) + F(y) \quad (8)$$

whose additive term is defined as

$$F(y) \equiv \frac{g''}{2g} - \frac{3}{4} \left(\frac{g'}{g} \right)^2 \quad (9)$$

Hereafter, a prime ($'$) symbol denotes differentiation with respect to our new radial variable y .

It should be noted that:

1. the modified wave function $\phi(y)$ is now defined on the finite domain $[a, b]$;
2. the modified radial equation (7) is completely equivalent to the initial one (2), as long as $r(y) \in (C^3[a, b])$ is a monotonically increasing function;

3. a knowledge of the inverse analytical function $r(y)$ is all that is required to accomplish the exact transformations of Eqs. (6)-(9);
4. for a fixed mesh of equally spaced y points on the interval $y \in [a, b]$, the function $\rho(r) = dy/dr = 1/g(y)$ defines the density distribution of mesh points of the initial coordinate r .

It is clear that conventional finite-difference [21, 23, 24, 26] and pseudospectral [22] methods can be used straightforwardly for integrating the transformed radial equation (7) out to the point $y = b$, as long as the modified wave function $\phi(y)$ is not singular anywhere on the interval $[a, b]$, and especially not at its end points. Furthermore, it will be proved in the next section that the scattering length a_s is an explicit function of logarithmic derivative of the wave function $\phi(y)$

$$\xi(y) \equiv \frac{\phi'(y)}{\phi(y)} \quad (10)$$

at the boundary $y = b$. It is well-known that the transformation (10) converts the radial equation (7) into the modified Riccati equation

$$\xi'(y) + \tilde{Q}(y) + \xi^2(y) = 0 \quad (11)$$

which can be numerically integrated, for instance, using Johnson's efficient log-derivative method [23, 24]. More details regarding this method are given in the Appendix.

B. Developing a Formula for the Scattering Length

Since Eq. (4) shows that the scattering length can be expressed formally in terms of the asymptotic behavior of the ordinary radial wavefunction $\psi(r)$, we can write

$$a_s \simeq r - \frac{\psi(r)}{d\psi(r)/dr}, \quad r \rightarrow \infty. \quad (12)$$

It therefore seems desirable to investigate the asymptotic behavior of the modified function $\phi(y)$ near the outer boundary point $y = b$ corresponding to $r \rightarrow \infty$, where

$$\phi(y) \simeq S \frac{r(y) - a_s}{\sqrt{dr(y)/dy}}, \quad y \rightarrow b. \quad (13)$$

Since we are mapping an infinite interval onto a finite one, it is clear that the mapping function $r(y)$ must have a singularity at the upper end of the interval. To proceed, we assume that this singularity has the form

$$r(y) \sim \frac{1}{(b-y)^\gamma}, \quad y \rightarrow b, \quad (14)$$

where necessarily $\gamma > 0$, because the $r(y)$ function must go to infinity as y approaches b in order to convert the finite domain $y \in [a, b]$ into the infinite one $r \in [r_{\min}, +\infty]$.

Inserting Eq. (14) into Eq. (13) yields

$$\phi(y) \simeq S (b-y)^{\frac{1-\gamma}{2}}, \quad y \rightarrow b \quad (15)$$

and differentiating that result with respect to y yields

$$\phi'(y) \simeq S \frac{1-\gamma}{(b-y)^{\frac{1+\gamma}{2}}}, \quad y \rightarrow b. \quad (16)$$

From Eqs.(15) and (16) it is immediately clear that for both the modified wave function $\phi(y)$ and its derivative $\phi'(y)$ to be non-singular at the point $y = b$ (or $r = +\infty$), necessarily $\gamma = 1$.

Avoidance of this singularity at $y = b$ is clearly desirable if we are to integrate the modified radial equation (7) accurately on the whole interval $[a, b]$, so it is necessary to choose a mapping function $r(y)$ that has only a simple pole at the end point $y = b$. Let us assume that $r(y)$ can be expressed as a Laurent series expansion about this point:

$$r(y) = \frac{c_{-1}}{b-y} + c_0 + \sum_{i=1}^{\infty} c_i (b-y)^i \quad (17)$$

where $c_{-1} > 0$. Inserting Eq. (17) into Eq. (13) and differentiating the resulting expression for $\phi(y)$ with respect to y yields, at the point $y = b$,

$$\phi(b) = S \sqrt{c_{-1}}, \quad \phi'(b) = \frac{S(a_s - c_0)}{\sqrt{c_{-1}}}, \quad (18)$$

which shows that

$$a_s = c_{-1} \xi(b) + c_0 \quad (19)$$

is the desired relationship between the scattering length a_s and the log-derivative function at the outer end of the interval, $\xi(b)$.

To facilitate accurate calculation of the the required $\xi(b)$ value, it is desirable that the function $\tilde{Q}(y)$ of Eq. (8) be nonsingular at the end point $y = b$. It is easy to verify that the $F(y)$ contribution is nonsingular at $y = b$, since

$$F(b) = -\frac{3c_1}{c_{-1}} \quad (20)$$

Moreover, from Eq. (17) it is clear that in the limit $y \rightarrow b$ (or $r \rightarrow \infty$),

$$g(y) \equiv \frac{dr(y)}{dy} \simeq \frac{c_{-1}}{(b-y)^2} \propto r^2. \quad (21)$$

This means that for any potential which dies off more slowly than $1/r^4$, the product $g^2 U(r)$ that comprises the main part of the function $\tilde{Q}(y)$ (see Eq. (8)) diverges in the limit $y \rightarrow b$ ($r \rightarrow +\infty$). In particular, if $U(r \rightarrow \infty) \simeq -C_n/r^n$, then as $y \rightarrow b$,

$$g^2 U(y) \simeq \frac{2\mu}{\hbar^2} \frac{C_n (b-y)^{n-4}}{(c_{-1})^{n-2}}, \quad (22)$$

and hence

$$\tilde{Q}(b) = \begin{cases} F(b) & n > 4 \\ \frac{2\mu}{\hbar^2} \frac{C_n}{(c_{-1})^2} + F(b) & n = 4 \\ \infty & n < 4 \end{cases}$$

This means that, to calculate the modified wavefunction $\phi(y)$ and/or its derivative $\phi'(y)$ at the end of the range ($y = b$) for an $n = 4$ case requires explicit knowledge of the leading long-range induction coefficient C_4 , while for the more common $n = 5$ or 6 cases it requires only a knowledge of the mapping function $r(y)$ that defined $F(b)$. In contrast, for $n < 4$ no satisfactory determination of $\phi(b)$ and/or $\phi'(b)$ can be achieved using the present approach. This latter result is consonant with the fact that the scattering length is not defined for potentials that die off more slowly than $1/r^4$ [1].

C. Introduction of Mapping Functions

To make practical use of our relationship (19) between the scattering length and the log-derivative function, it is necessary to introduce an analytical mapping function with the Laurent expansion form of Eq. (17). The simplest way to do this is to define the mapping function as the first two terms of the Laurent series:

$$r(y) = \frac{c_{-1}}{b-y} + c_0, \quad (23)$$

since only the c_{-1} and c_0 coefficients are required in Eq. (19). In particular, setting $b = 1$ and $c_{-1}/2 = -c_0 \equiv \bar{r}$, in (23) yields a version of (omitting a factor of 2) of the well-known Ogilvie-Tipping (OT) potential energy expansion variable [19]:

$$y_{\text{OT}}(r; \bar{r}) = \frac{r - \bar{r}}{r + \bar{r}}; \quad y_{\text{OT}} \in [-1, 1]. \quad (24)$$

For this case Eq. (19) shows that the scattering length is explicitly defined as

$$a_s = \bar{r} [2\xi(1) - 1] \quad (25)$$

while the reciprocal mapping function is

$$r_{\text{OT}}(y) = \bar{r} \left(\frac{1+y}{1-y} \right) \quad (26)$$

and

$$g_{\text{OT}}(y) = \frac{2\bar{r}}{(1-y)^2} = \frac{(r + \bar{r})^2}{2\bar{r}} \quad (27)$$

Moreover, for this mapping function the additive term $F_{\text{OT}}(y) = 0$.

Use of the simple one-parameter mapping function of Eq. (24) does provide a reliable method for calculating a_s . However, our recent experience with applying this type

of transformation to bound-state problems [18] suggests that better efficiency may be attained using more flexible two-parameter functions. One such function which was successfully used for bound-state calculations is the two-parameters ($\bar{r}, \alpha > 0$) Šurkus variable [20]:

$$y_S(r; \bar{r}, \alpha) = \frac{r^\alpha - \bar{r}^\alpha}{r^\alpha + \bar{r}^\alpha}; \quad y_S \in [-1, 1] \quad (28)$$

for which the reciprocal mapping function is

$$r_S(y) = \bar{r} \left(\frac{1+y}{1-y} \right)^{1/\alpha} \quad (29)$$

However, except for the special case $\alpha = 1$ in which $y_S(r; \bar{r}, \alpha)$ reduces to $y_{\text{OT}}(r; \bar{r})$, this mapping function is not appropriate for scattering-length calculations, since when $\alpha \neq 1$ the mapping function $r_S(y)$ does not take on the required Laurent series expansion form (17) as $y \rightarrow 1$, so the associated log-derivative wavefunction $\xi(y)$ becomes singular there.

In contrast, the two-parameters tangential function [22]

$$r_{\text{tg}}(y) = \bar{r} \left[1 + \frac{1}{\beta} \tan \left(\frac{\pi y}{2} \right) \right] \quad (30)$$

defined on the interval $y \in [(2/\pi) \tan^{-1}(-\beta), 1]$, whose inverse is the inverse tangent function

$$y_{\text{tg}}(r; \bar{r}, \beta) = \frac{2}{\pi} \tan^{-1} [\beta (r/\bar{r} - 1)] \quad (31)$$

completely conforms to the required Laurent expansion form of Eq. (17) as $y \rightarrow 1$, since

$$r_{\text{tg}}(y) \simeq \frac{2\bar{r}}{\pi\beta(1-y)} + \bar{r} - \frac{\pi\bar{r}}{6\beta}(1-y) + \dots \quad (32)$$

For this case

$$a_s = \bar{r} \left[\frac{2\xi(1)}{\pi\beta} + 1 \right], \quad (33)$$

and it is easy to show that the additive contribution to Eq. (8) is a constant,

$$F_{\text{tg}}(y) = \frac{\pi^2}{4}, \quad (34)$$

and that

$$\begin{aligned} g_{\text{tg}}(y) &= \frac{\pi\bar{r}}{2\beta} \cos^{-2}(\pi y/2) \\ &= \frac{\pi\bar{r}}{2\beta} \left[1 + \beta^2 (r/\bar{r} - 1)^2 \right]. \end{aligned} \quad (35)$$

D. Determination of Optimal Mapping Parameters

The optimal values of the parameters defining the mapping function of Eq. (30) may be expected to depend both on the nature of the interaction potential $U(r)$ and on the particular numerical method used for integration of

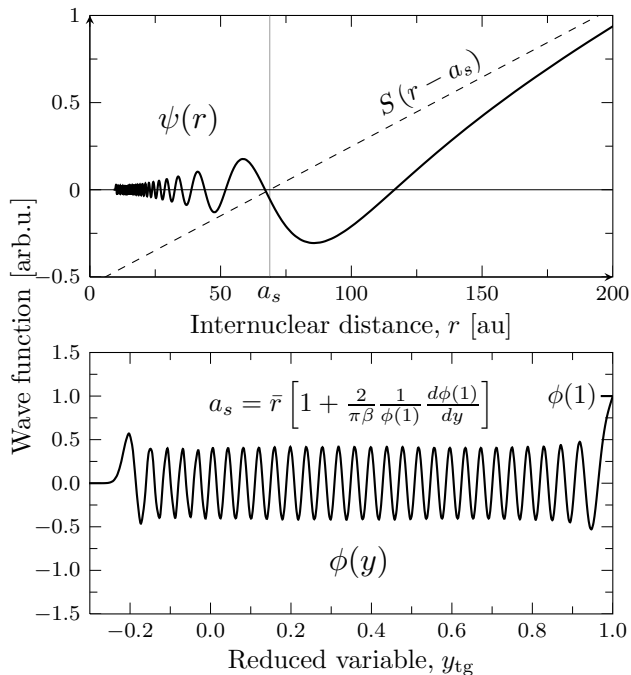


FIG. 1. Comparison of the original $\psi(r)$ and modified $\phi(y) = \psi/\sqrt{g_{\text{tg}}}$ unbound wave functions at zero energy for the $a^3\Sigma_u^+$ state of Cs_2 [15], as calculated using the Numerov method [21, 29]. The scaling function $g_{\text{tg}}(r)$ was calculated from Eq. (35) using the mapping parameters $\bar{r} = r_e = 12.0$ [au] and $\beta = 2$.

the modified radial equation (7). When using Johnson's log-derivative method of integration [23, 24], the optimal mapping parameters \bar{r} and β could be determined by minimizing the truncation error $\Delta\xi$ estimated using a Richardson extrapolation (RE) (A.7), or by minimizing the difference between $\xi_{h_1}(y = b)$ and $\xi_{h_2}(y = b)$ values corresponding to two different integration step sizes h_1 and h_2 ,

$$\min |\xi_{h_1} - \xi_{h_2}|. \quad (36)$$

Note that it is tacitly assumed that the optimal parameter values do not depend on the integration step size. This has been confirmed by the illustrative calculations presented in Section III. It will also be shown there that the minimum of the functional (36) is a rather smooth function of both mapping parameters, \bar{r} and β .

It seems reasonable to assume that the optimal mapping function would correspond to the situation in which

$$\tilde{Q}(y) \equiv g^2(y) Q(r(y)) + F(y) \approx \text{const} \quad (37)$$

since it is well-known that minimal truncation errors arise in particle-in-a-box problems where the potential $U(r)$ does not depend on r . Furthermore, within the classically allowed region where $Q \gg 0$, the additive term $F(y)$ can be approximately neglected [1, 16]. In this case Eq. (37) reduces to $g^2 Q \approx \text{const}$, and inverting this condition (recalling that $g(y) \equiv dr/dy$) yields

$$y_{\text{opt}}(r > r_0) \sim \int_{r_0}^r \sqrt{Q(r)} dr \quad (38)$$

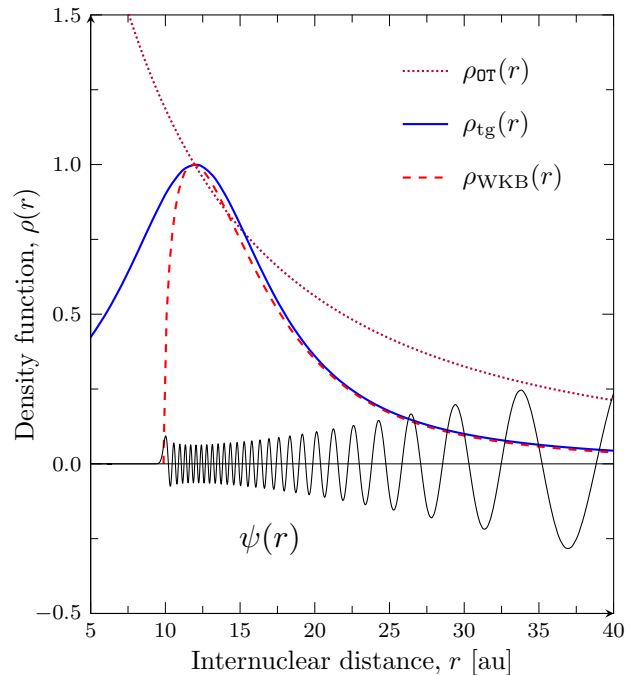


FIG. 2. (Color online) Mapping density functions $\rho(r) = dy/dr = 1/g(r)$ for the $a^3\Sigma_u^+$ state of Cs_2 [15] calculated: (i) within the framework of the conventional WKB approximation $\rho_{\text{WKB}} = \sqrt{-U(r)}$ (39), (ii) using the one-parameter $y_{\text{opt}}(r; \bar{r})$ mapping function (24) with $\bar{r} = r_e = 12.0$ [au], and (iii) using the two-parameters $y_{\text{tg}}(r; \bar{r}, \beta)$ mapping function (31) with $\bar{r} = r_e$ and $\beta = 2$. $\psi(r)$ is the associated zero-energy wavefunction.

Here r_0 is the left-hand (inner) classical turning point, which is the root of the equation $U(r_0) = 0$.

Differentiating Eq. (38) with respect to r yields

$$\rho_{\text{opt}} \equiv \frac{dy_{\text{opt}}}{dr} \sim \sqrt{Q(r)} \equiv \sqrt{-\frac{2\mu}{\hbar^2} U(r)} \quad (39)$$

For optimal mapping, therefore, the density function $\rho_{\text{opt}}(r)$ should be close to $\sqrt{Q(r)}$ in the $Q(r) \gg 0$ region where the original wavefunction $\psi(r)$ has its maximum oscillation frequency. From Eq. (39) it follows that the optimal mapping does not depend on the reduced mass μ , because it appears in $Q(r)$ simply as a multiplicative factor. It is also easy to see that the mapping function (38) transforms the modified wavefunction $\phi(y)$ into the familiar particle-in-a-box form

$$\phi_{\text{opt}}(y) \sim A \sin(ky) + B \cos(ky) \quad (40)$$

which correlates with the conventional WKB approximation [1, 16] in the classically allowed region where $Q(r) > 0$. As is shown by Fig. 1, in contrast to the original wavefunction $\psi(r)$, the modified wavefunction $\phi(y)$ has loops of almost constant amplitude and spacing over the potential well, behavior which is qualitatively very similar to that implied by Eq. (40). It is therefore expected that the WKB mapping of Eq. (38) should be close to ‘‘optimal’’ for all numerical methods (such as the

finite-difference and collocation methods) that are based on an equidistant grid in the classical region of motion. It should be stressed, however, that the mapping function defined by Eq. (38) cannot itself be applied for scattering length calculations because it does not satisfy the required asymptotic behavior of Eq. (17), and because it becomes imaginary in the classically forbidden region where $r < r_0$.

It is easy seen from Eqs. (27) and (35) that the density function $\rho_{\text{OT}}(r)$ corresponding to the one-parameter mapping function of Eq. (24) is proportional to $1/[r+\bar{r}]^2$, while that for the two-parameters tangent function of Eq. (31) has a Lorentzian form with a maximum at \bar{r} . The plots presented in Fig. 2, show that there is good agreement between the $\rho_{\text{WKB}}(r)$ and $\rho_{\text{tg}}(r)$ density functions over much of the domain of the wavefunction $\psi(r)$. This leads to the conclusion that the optimal value of parameter \bar{r}_{opt} should be close to the equilibrium inter-nuclear distance r_e of the potential $U(r)$. Hence, for the two-parameters mapping function (31), it seems reasonably to fix $\bar{r}_{\text{opt}} \approx r_e$ and to vary only the single parameter β . Note that the pronounced differences among the density functions for these three cases at small distances is not very important, because the associated wave function $\psi(r)$ dies off exponentially in this region.

In the following, therefore, parameter \bar{r} of the mapping functions $y_{\text{OT}}(r; \bar{r})$ of Eq. (24) and $y_{\text{tg}}(r; \bar{r}, \beta)$ of Eq. (31) is fixed as $\bar{r} = r_e$, while the optimum value of β of Eq. (31) is determined from a one-dimensional minimization of the functional of Eq. (36).

III. IMPLEMENTATION, TESTING, AND DISCUSSION

A. Model-Potential Applications and Tests

A computer program based on the adaptive mapping procedure described above has been written and tested [29], both for a variety of model potentials, and on potentials for real systems taken from the literature. All results were obtained on 32 bit processors, mainly using double-precision arithmetic, but with quadruple-precision calculations being used sometimes in order to delineate the impact of accumulated numerical round-off error. This section presents the results of those illustrative applications, together with some general discussion of the method.

The first sample calculations presented here are for the model Lennard-Jones($2n, n$) potentials

$$U_{\text{LJ}}(r) = \mathfrak{D}_e \left[\left(\frac{r_e}{r} \right)^{2n} - 2 \left(\frac{r_e}{r} \right)^n \right]. \quad (41)$$

defined by the potential function parameters and system reduced mass listed in Table I. The first three of these LJ($2n, n$) potentials, each supporting 15 bound vibrational levels, are the same models systems considered in our recent application of this adaptive mapping approach

TABLE I. The s -wave scattering wavelengths a_s (in Å) calculated for the LJ($2n, n$) potentials defined by Eq.(41) [29]. All models have equilibrium distance $r_e = 1$ [Å] and the reduced mass is set as $\mu = 16.85762920$ [au] so that in “spectroscopists units”, the scaling factor $\hbar^2/2\mu = 1$ [$\text{cm}^{-1} \text{Å}^2$]. \mathfrak{D}_e is the well depth in cm^{-1} , while v_{max} is the vibrational quantum number of the last bound level supported by the potential.

n	v_{max}	\mathfrak{D}_e	β_{opt}	$\frac{n}{2} - 1$	a_s^\ddagger	a_s
4	14	1000	0.9	1.0	277.4	310.54293138289
5	14	2165	1.5	1.5	234.9	246.72686552846
6	14	3761	2.1	2.0	236.1	242.48308194261
6	99	176200	2.1	2.0		10.849479064634
6	99	174370	2.1	2.0		11552.057690297

[‡]The a_s estimates obtained using the last-level binding energy approximation of Eq.(5).

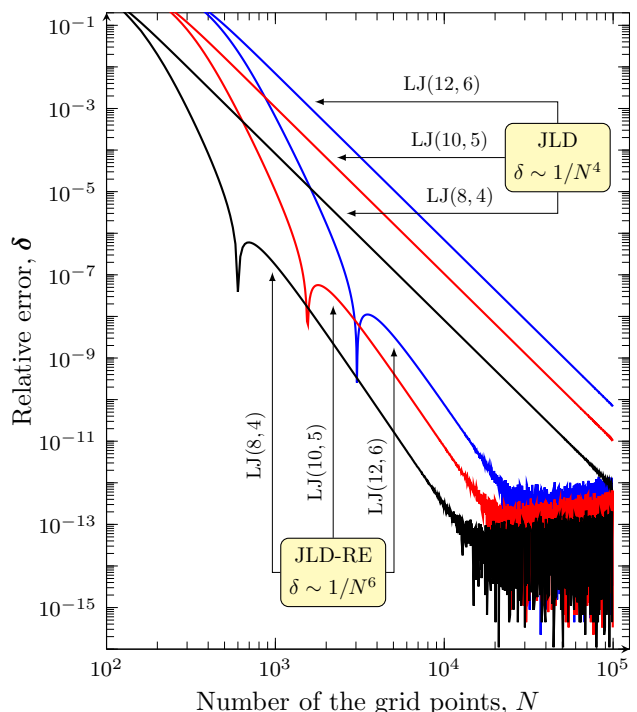


FIG. 3. (Color online) Convergence tests for a_s -values calculated in double precision arithmetic for the model 15-level LJ($2n, n$) potentials of Table I using the one-parameter mapping function $y_{\text{OT}}(r; \bar{r})$ (24) with $\bar{r} = r_e = 1$ [Å]. Calculations performed using Johnson’s log-derivative method alone are denoted ‘JLD’, while the results labeled ‘JLD-RE’ were obtained by also applying a $(N, N/2)$ -Richardson extrapolation procedure to those results.

to bound-state problems [18]. The last two LJ(12, 6) potentials have much deeper wells and support 100 vibrational levels. They were introduced here to highlight the efficiency of the present method, since the computational effort of scattering-length calculations increases dramatically as v_{max} and the absolute magnitude of a_s -values increase.

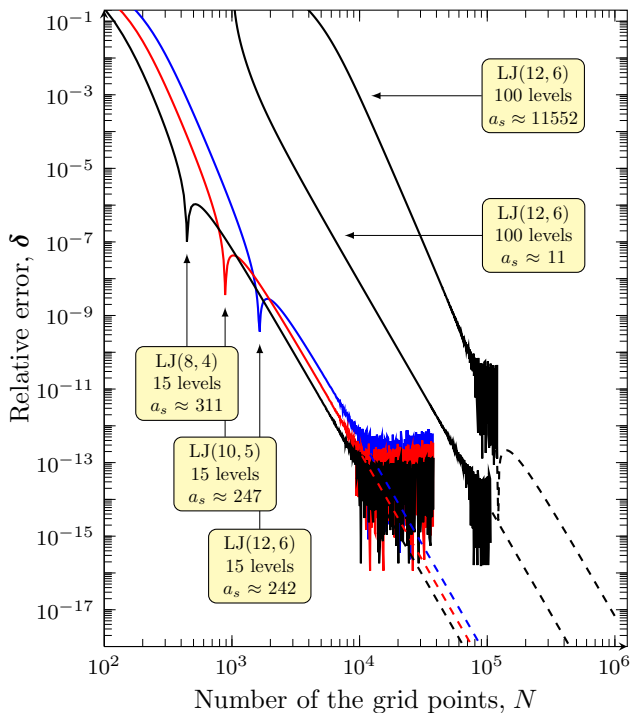


FIG. 4. (Color online) Convergence tests for a_s -values calculated by the JLD-RE($N, N/2$) method in double precision arithmetic (solid curves) for the five model LJ($2n, n$) potentials of Table I using the two-parameters $y_{tg}(r; \bar{r} = r_e, \beta)$ mapping function of Eq. (31) with the optimal parameters β_{opt} listed there. The dashed lines present results obtained using quadruple-precision arithmetic.

Converged a_s -values for five model LJ($2n, n$) potentials are presented in the last column of Table I. As discussed above, the range-mapping parameter was fixed at $\bar{r} = r_e = 1[\text{\AA}]$ for both $y_{\text{OT}}(r)$ and $y_{\text{tg}}(r)$ mapping functions. The optimal β_{opt} values for the latter case were determined by minimizing the functional of Eq. (36), yielding the results shown in the column four. It is interesting to see that these empirically determined β_{opt} values have essentially the same dependence on the inverse-power n governing the long-range behavior of the potential as was the case for the analogous parameter α of the Šurkus-variable mapping (28) used in the bound-state study of Ref. [18].

The log-log plots in Figs. 3 and 4 show how the relative errors in the calculated a_s values

$$\delta = \left| \frac{a_s^{\text{calc}}}{a_s^{\text{exact}}} - 1 \right| \quad (42)$$

depend on the number of mesh points N used in the radial integration. The reference values a_s^{exact} were obtained from calculations using quadruple precision arithmetic by increasing N until the full desired level of convergence was achieved. The numerical ‘noise’ on these plots for $\delta \lesssim 10^{-12}$ indicates the precision limits achieved using ordinary double-precision arithmetic, while the

dashed lines show how the convergence trend continues when quadruple-precision arithmetic is used.

The three upper curves in Fig. 3 (labeled JLD) display results obtained using Johnson’s log-derivative method, while the three lower curves illustrate the greatly improved convergence achieved when that approach is coupled to the ($N, N/2$) Richardson extrapolation procedure described in the Appendix. These results clearly confirm the prediction of Eq. (A.5), that Johnson’s log-derivative method (JLD), and that method combined with a Richardson extrapolation to zero step (JLD-RE), demonstrate N^{-4} and N^{-6} convergence rates, respectively. We see that for these 15-level LJ potentials, the JLD-RE($N, N/2$) method allows us to attain 11-12 significant digits in calculated a_s values when using only $N \approx 10^4$ radial mesh points.

The results displayed in Fig. 4 show that as expected, the computational effort increases significantly for the 100-level LJ($2n, n$) models, especially for the very last case considered in Table 1, for which the scattering length is extremely large: $a_s \approx 10^4 [\text{\AA}]$. However, that even for those cases full double-precision converge is achieved with only $N \approx 10^5$. Note that for a given number of grid points, use of the simple one-parameter mapping function $y_{\text{OT}}(r)$ yields relative errors that are only ~ 10 times larger than the analogous results yielded by the optimum two-parameter functions $y_{\text{tg}}(r)$. The non-linear ‘cusp’-like behavior near $N \approx 10^3$ on the JLD-RE plots in Figs. 3 and 4 appears to be due to accidental cancellation of higher-order terms in the RE series expansion for these cases. It does not appear in analogous results based on use of a Numerov propagator.

The results presented in Fig. 5 clearly show that the accuracies of a_s values calculated with any given number of mesh points N vary smoothly with the value of mapping parameter parameter β . They also show that the optimal parameter value β_{opt} is essentially independent of the number of integration points used. Analogous results are obtained when modeling LJ($2n, n$) potentials with $n = 4$ and 5.

The sensitivity of the value of β_{opt} to the depth of the potential energy well has also been investigated. Figure 6 shows that the values of β_{opt} for model LJ($2n, n$) potentials only depend significantly on the dissociation energy \mathcal{D}_e for very shallow potentials which support only a few bound states. For such species (e.g., see the He₂ example considered below), accurate scattering lengths can readily be calculated using a relatively small number of grid points, so determining precise values of β_{opt} is immaterial. Overall, Fig. 6 shows that the optimal value of the β parameter in the mapping function of Eq. (31) depends mainly on the inverse-power n governing the limiting long-range behavior of the interaction potential. As indicated by Fig. 6 and Table I, these optimal values are approximately defined by the simple relationship

$$\beta_{\text{opt}} \approx \frac{n}{2} - 1, \quad (43)$$

at least for these LJ($2n, n$)-like potentials. We believe

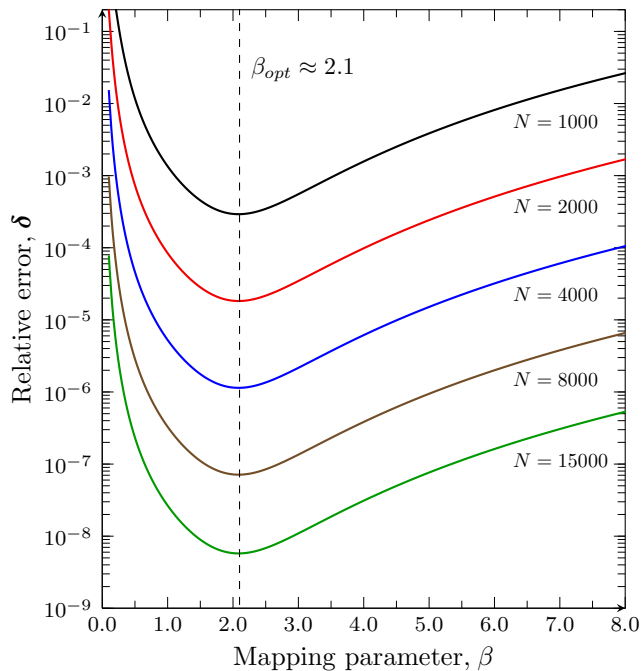


FIG. 5. (Color online) Relative errors (42) in the a_s -values obtained for the 15-level LJ(12, 6) potential (41) as functions of the mapping parameter β , where N is the number of grid points used in the JLD method.

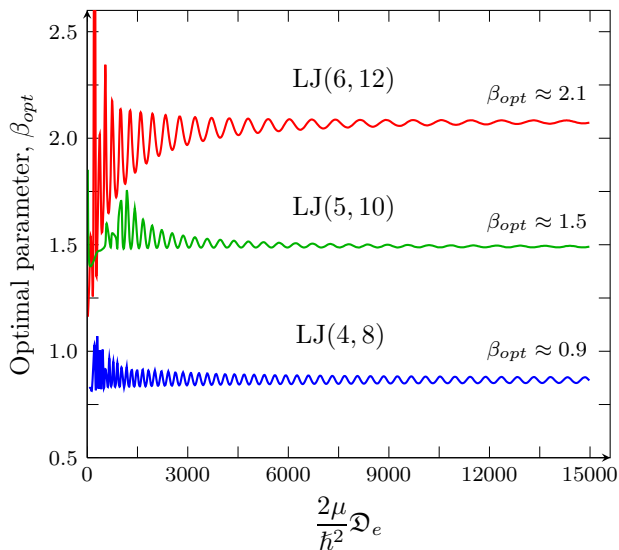


FIG. 6. (Color online) Optimal mapping parameter β_{opt} as a function of the dissociation energy \mathcal{D}_e of 15-level LJ($2n, n$) potentials (41) for $n = 4, 5$ and 6 .

that this empirical rule will be valid when applying the two-parameter mapping function of Eq. (30) to any deeply bound interatomic potential having a long-range tail which dies off as $1/r^n$ for $n \geq 4$.

It is interesting to note that the two-parameters mapping function $y_{\text{tg}}(r; \bar{r}, \beta)$ of Eq. (31) is also well suited for solving the Schrödinger equation for the bound-state

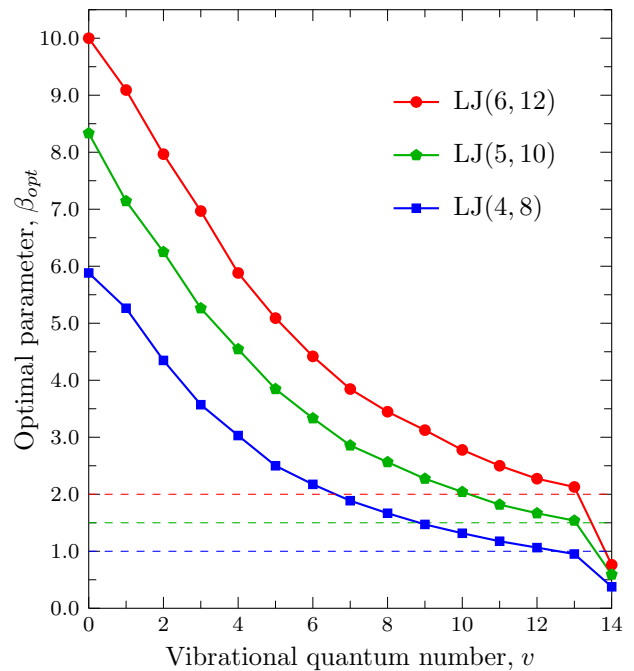


FIG. 7. (Color online) Optimal mapping parameters β_{opt} determined for the bound vibrational levels $v \in [0, 14]$ of the model 15-level LJ($2n, n$) $n=4, 5, 6$ potentials (41). The dashed horizontal lines corresponds to the β_{opt} values implied by Eq.(43).

problem discussed in Ref. [18]. In particular, Fig. 7 shows how the values of β_{opt} evolve if this mapping parameter is optimized independently for each level of our three 15-level LJ($2n, n$) potentials. Except for the very last level, the values of β_{opt} smoothly approach the limiting value implied by Eq. (43) as the vibrational levels approach dissociation. The substantial deviation from this limiting behavior for the lower vibrational levels is not a matter of concern, since those levels can readily be located accurately using a very wide range of β values, and since their radial amplitude is much smaller than that for the highest levels, the overall computational efficiency for such levels is not very strongly dependent on the value of β . The abrupt drop-off in the values of β_{opt} for the very last level also mimics the behavior found in Ref. [18] using very different mapping functions (29) based on the Šurkus variable [20] defined by Eq.(28). This abrupt decrease of β_{opt} for the last very weakly bound vibrational level $v = v_{\text{max}} = 14$ is related to the form of the corresponding wavefunction $\psi_{v_{\text{max}}}(r)$ which has very broad last loop centered at a very large internuclear distance. In particular, for the case of a last level which lies extremely close to dissociation, it appears that a small limiting value of $\beta_{\text{opt}} \lesssim 0.5$ is needed to provide a sufficiently broad distribution of grid points to properly characterize the outermost loop of the wavefunction.

B. Applications to ‘Real’ Systems

This section describes application of our new method of performing scattering length calculations to three ‘real’ physical problems. The first of these is the elastic scattering of a free electron from a neutral Xe atom. The function used for the Xe–e[−] interaction potential is the ‘HFD’-type potential reported by Szmytkowski [13] (with energy and distance in atomic units):

$$U_{\text{Xe-e}^-}(r) = A e^{-\gamma r^2} - \sum_{n=4,6} F_n(r) C_n / r^n, \quad (44)$$

in which $A = 306.0$ and $\gamma = 1.0$, while the n -dependent damping function F_n has the form

$$F_n(r) = \left[1 - e^{-(r/r_c)^2} \right]^n \quad (45)$$

with $r_c = 1.89$ being a cut-off radius, such that $F_n(r) = 0$ for $r < r_c$. Following Czuchaj *et al.* [27], its dispersion coefficients $C_4 = \alpha_1/2$ and $C_6 = (\alpha_2 - 6\beta_1)/2$ in Eq.(44) correspond to the familiar charge/induced-dipole and charge/induced-quadrupole interactions, where $\alpha_1 = 27.292$ and $\alpha_2 = 128.255$ are the static dipole and quadrupole polarizabilities of the Xe atom, while $\beta_1 = 29.2$ is the dynamical correction to the dipole polarizability. This shallow $U_{\text{Xe-e}^-}(r)$ interaction potential supports no bound levels and its scattering length is negative, as was determined by Szmytkowski using an asymptotic method [13].

The present a_s -value for this system (in au), given in the first row of Table II, was converged to 14 significant digits using the JLD-RE($N,N/2$) method based on $N \approx 10^3$ grid points and a scaling factor of $\hbar^2/2\mu = 0.5$. However, only $N \approx 100$ grid points are required to converge the present a_s -value to 7 significant digits. The present estimate agrees with the value reported by Szmytkowski [13] to within the 6 significant digit that he reports (see row 2 of Table II).

Our second real-world example is a modified ‘Hartree-Fock dispersion’ (HFD) type potential for the $a^3\Sigma_u^+$ ground triplet state of the cesium dimer [12, 13, 15] (again, with energies and distances in atomic units):

$$U_{\text{Cs}_2}(r) = A r^\alpha e^{-\gamma r} - F(r) \left[\sum_{n=6,8,10} C_n / r^n \right]. \quad (46)$$

The first term in Eq.(46), defined by constants $A = 8 \times 10^{-4}$, $\alpha = 5.53$ and $\gamma = 1.072$, represents the exchange repulsion energy, while the second is a sum of van der Waals dispersion terms (with coefficients $C_6 = 7.02 \times 10^3$, $C_8 = 1.1 \times 10^6$, $C_{10} = 1.7 \times 10^8$) multiplied by the n -independent damping function

$$F(r) = H(r - r_c) + H(r_c - r) e^{-(r_c/r-1)^2} \quad (47)$$

where $H(x)$ is the Heaviside step function: $H(x) = 1(0)$, when $x \geq (<)0$, while $r_c = 23.165$ is the cut-off radius. This potential energy function supports up to 58

TABLE II. Comparison of s -wave scattering lengths a_s (in au) obtained in the framework of JLD-RE($N,N/2$) procedure [29] using realistic published potentials for Xe–e[−] [27], Cs₂($a^3\Sigma_u^+$) [12, 13, 15], and ^{3,4}He₂($X^1\Sigma_g^+$) [28] interactions and two-parameter mapping function $y_{\text{tg}}(r; \bar{r}, \beta)$ of Eq. (31). The optimal mapping parameters β_{opt} were determined by minimization of the functional (36), while the \bar{r} values (in au) were fixed at $\bar{r}_{\text{opt}} = r_e$, where r_e is the equilibrium distance of the relevant potential.

species	potential	n	v_{max}	a_s	β_{opt}	\bar{r}_{opt}
Xe–e [−]	Eq. (44)	4	‡	−4.95280521509712	1.7	3.2
				−4.95281 ^a		
Cs ₂	Eq. (46)	6	57	68.215967213	2.0	12.0
				68.21596 ^b		
				68.21823 ^a		
				68.0 ^c		
⁴ He ₂	Eq. (48)	6	0	236.3688418603	2.5	5.67
				236.36884174 ^d		
³ He ₂			‡	−13.17845206095	3.6	5.67
				−13.178452062 ^d		

‡There are not bound levels.

^a Ref. [13]

^b Ref. [12]

^c Ref. [15]

^d Ref. [11]

bound levels, and can be considered a typical example of a many-level interatomic potential.

The present a_s -value, obtained using our JLD-RE($N,N/2$) procedure with a scaling factor of $\hbar^2/2\mu = 1/2.422 \times 10^5$, is listed in row 3 of Table II. It agrees with previous estimates obtained using WKB [15] (row 6), asymptotic [13] (row 5), and iterative [12] (row 4) methods to within 2, 4 and 7 significant digits, respectively. The present method required about $N \approx 10^4$ grid points to obtain 10 significant digits in the calculated a_s -value.

Our third practical application is to the ground $X^1\Sigma_g^+$ state of the helium dimer, for which the interaction potential is again represented by an ‘HFD’-type function [28] written as (with energies in K and distances in Å)

$$U_{\text{He}_2}(r) = \mathfrak{D} \left[A \exp(-\gamma x) - F(x) \left(\sum_n \frac{C_n}{x^n} \right) \right], \quad (48)$$

in which $x = r/r_m$, $\mathfrak{D} = 10.8$, $A = 544850.4$, $\gamma = 13.353384$, $C_6 = 1.3732412$, $C_8 = 0.4253785$, $C_{10} = 0.1781$, and $r_m = 2.9673$. The damping function $F(x)$ in Eq. (48) is defined by Eq.(47) with the parameter $x_c = r_c/r_m = 1.28$. This is an exotic example of very shallow interatomic potential, as it supports only a single bound level for the heavier isotopologue ⁴He₂ and no bound levels at all for the lighter isotopologue ³He₂. For consistency with the calculations of Ref. [11], the values of the scaling factors $\hbar^2/2\mu$ used in the present calculation were 16.085775 and 12.120904 for ³He₂ and ⁴He₂, respectively.

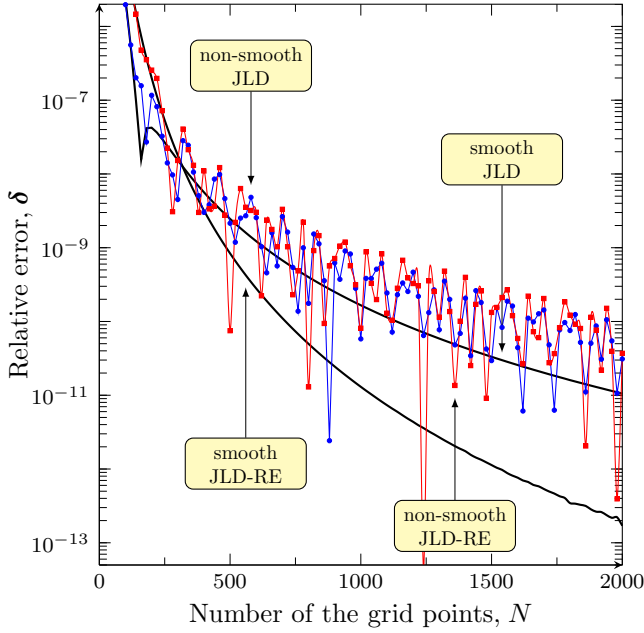


FIG. 8. (Color online) Comparison of convergence behavior for scattering lengths implied by the ${}^3\text{He}_2(X^1\Sigma_g^+)$ potential [28] as calculated by the JLD(N) and JLD-RE($N, N/2$) procedures using smooth *vs* non-smooth long-range damping functions of Eq. (47).

The results presented in the last four rows of Table II show that the present a_s -values (first entry for each case) agree with the result obtained in Ref.[11] using the asymptotic method to about 10 significant digits. However, the JLD-RE($N, N/2$) procedure used here required only $N = 100$ grid points to obtain a_s -values for both isotopologues with uncertainties of only 0.01%.

An interesting general point concerns the fact that the convergence behavior of the a_s -values calculated for Cs_2 and He_2 at high N was not as smooth as it was for the model LJ($2n, n$) and realistic Xe-e^- potentials; this is demonstrated by the contrast between the curves in Fig. 4 and the 'non-smooth' curves in Fig. 8. We attribute this behavior to the discontinuous second and higher derivatives of the damping function $F(x)$ in the potentials of Eqs. (46) and (48), at the point $r = r_c$. To confirm this assertion, the a_s calculations for ${}^3\text{He}_2$ were repeated with the Heaviside switching function of Eq. (47) replaced by the smooth switching function

$$\tilde{H}(x) = \frac{1}{1 + e^{-2kx}}; \quad k = 10 \quad (49)$$

The results obtained in this way, plotted as the 'smooth' curves in Fig. 8, clearly confirm our assertion. This demonstrates the importance of having potential energy functions models which have a very high degree of analytic smoothness.

Our final point concerns the sensitivity of the calculated a_s -values to the position of the inner boundary $r_{\min}(y = a)$ of the integration region. While the trans-

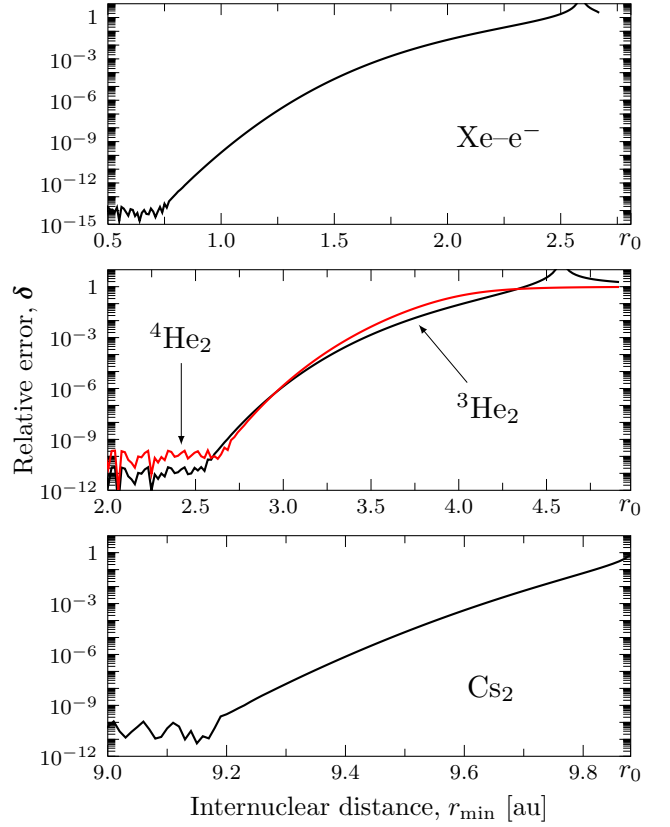


FIG. 9. (Color online) Convergence of calculated scattering lengths for the Xe-e^- , ${}^{3,4}\text{He}_2(X^1\Sigma_g^+)$, and $\text{Cs}_2(a^3\Sigma_u^+)$ systems with respect to the lower bound of the integration interval, r_{\min} , where r_0 is the distance where $U(r) = 0$.

formation of Eqs. (30) and (31) formally fixes the lower bound for $y_{\text{tg}}(r)$ to correspond to $r = 0$, the exponentially rapid decay of the wavefunction in the classically forbidden region under the short-range repulsive potential wall means that in practice that lower bound may be set quite a bit closer to the left turning point r_0 where $U(r) = 0$. To examine this point, Fig. 9 shows the convergence behavior of calculated values of a_s for the three real systems of Table II as the lower limit of the integration interval is shifted inward from the distance r_0 . It was found that values of r_{\min} for which the relative error approaches the double-precision numerical-noise limit can be defined by the criterion

$$(r_{\min} - r_0) \times \sqrt{\frac{2\mu}{\hbar^2} |U(r_{\min})|} \gtrsim 23, \quad (50)$$

which is based on semi-classical exponential decay of the original $\psi(r)$ wavefunction in the classically forbidden region by a factor of $\sim 10^{-10}$. For the $y_{\text{tg}}(r; \bar{r}, \beta)$ mapping function of Eq.(31), this implies an inner (left hand) boundary point of $a = \frac{2}{\pi} \tan^{-1} [\beta (r_{\min}/\bar{r} - 1)]$.

IV. CONCLUSIONS

This paper presents a very robust and efficient new way of calculating scattering lengths. The two-parameter mapping function of Eq. (30) transforms the conventional radial Schrödinger equation (2) into the equivalent form of Eq. (7) defined on the finite domain $y \in [a, 1]$. For arbitrary interaction potentials, neither the solution $\phi(y)$ of the transformed equation nor its first derivative $\phi'(y)$ are singular anywhere on this interval. As a result, the s -wave scattering length a_s can be exactly expressed in terms of the logarithmic derivative of this transformed wave function $\phi(y=1)$ at the right boundary point, as specified by Eq. (33). The method does not depend on a particular asymptotic form of the potential as long as it dies off as fast as $1/r^n$ for $n \geq 4$, as $r \rightarrow \infty$.

For well-bound potentials with equilibrium distance r_e and a limiting (attractive) long-range behavior of $1/r^n$, the optimal values of the $y_{\text{tg}}(r)$ mapping parameters have been shown to be $\bar{r} \approx r_e$ and $\beta \approx \frac{n}{2} - 1$, respectively. These same mapping parameters also yield efficient solutions when this approach is used for solving bound-state problems. Regardless of the absolute magnitude of the scattering length or the number of bound levels supported by the potential, the accuracy of the a_s calculation can easily achieve 10-12 significant digits when working in ordinary double-precision arithmetic. It is also shown that stable and highly precise values of a_s cannot be determined for analytical potentials which lack high-order analytic smoothness throughout the classically allowed region. A computer program applying this approach has been submitted to the Journal's online data archive [29].

Finally, we note that although it requires a little more computational effort to achieve a given level of precision, combination of the $y_{\text{OT}}(r)$ mapping function of Eq. (24) with a conventional Numerov wavefunction propagator [21] can yield both accurate a_s values and wavefunctions $\phi(y)$ that can be used for calculating photoassociation cross sections and other properties [30].

ACKNOWLEDGMENTS

This work has been supported by the Russian Foundation for Basic Research by grant 10-03-00195a, and by NSERC Canada. The Moscow team is also grateful for partial support from the Federal Program "Scientists and Educators for an Innovative Russia 2009-2013", contract

P 2280.

Appendix: Johnson's log-derivative method

As was shown in Refs. [23] and [24], Johnson's quadrature procedure for outward integration of the Riccati equation (11) is based on the two-point finite-difference scheme:

$$z_k = \frac{z_{k-1}}{1 + z_{k-1}} - \left(\frac{h^2}{3}\right) w_k u_k, \quad (\text{A.1})$$

where $\xi_k(y_k) = h^{-1} z_k(y_k)$, the mesh points are $y_k = a + kh$, the integration step is $h = (b - a)/N$, and

$$u_k = \begin{cases} \tilde{Q}(y_k) & k = 0, 2, 4, \dots, N \\ \frac{\tilde{Q}(y_k)}{1 + (h^2/6)\tilde{Q}(y_k)} & k = 1, 3, 5, \dots, N-1 \end{cases} \quad (\text{A.2})$$

with weights w_k as in a Simpson quadrature

$$w_k = \begin{cases} 1 & k = 0, N \\ 4 & k = 1, 3, 5, \dots, N-1 \\ 2 & k = 2, 4, 6, \dots, N-2 \end{cases} \quad (\text{A.3})$$

The total number of integration points must be odd, so N must be an even number.

In the classically forbidden region where $\tilde{Q}(y_0) < 0$, the initial value log-derivative solution $z_0 = z(a)$ can be estimated using the semi-classical approximation [16, 24]:

$$z_0 = h \left[\sqrt{-\tilde{Q}(y_0)} - \left(\frac{h}{3}\right) \tilde{Q}(y_0) \right] \quad (\text{A.4})$$

It has been verified by numerical calculations [24] that the cumulative truncation error of the log-derivative method is given by

$$\xi_{h \rightarrow 0} - \xi_h = Ch^4 + \mathcal{O}(h^6) \quad (\text{A.5})$$

As a result, an approximate solution $\xi_h(b)$ determined with fixed integration stepsize (or a fixed number of mesh points) $h_i(N_i)$ can be extrapolated to zero step size using Richardson's formula [25, 26]:

$$\xi_{h \rightarrow 0}(b) \simeq \xi_{h_1}(b) + \Delta\xi(b), \quad (\text{A.6})$$

where

$$\Delta\xi = \frac{\xi_{h_1} - \xi_{h_2}}{\lambda^4 - 1}; \quad \lambda \equiv \frac{h_2}{h_1} = \frac{N_1}{N_2}. \quad (\text{A.7})$$

-
- [1] L. D. Landau and E. M. Lifshitz, *Quantum Mechanics: Non-relativistic theory*, Pergamon Press (1965).
 [2] N. F. Mott and H. S. W. Massey, *The Theory of Atomic Collisions*, Oxford University Press (1965).
 [3] I. Bloch, J. Dalibard, and W. Zwerger, Rev. Mod. Phys.,

- 80**, 885 (2008).
 [4] J.M. Hutson and P.Soldan, Int. Rev. Phys. Chem., **25**, 497 (2006).
 [5] C. Pethick and H. Smith, *Bose-Einstein Condensation in Dilute Gases*, Cambridge University Press (2002).

- [6] L. S. Rodberg and R. M. Thaler, *Introduction to the Quantum Theory of Scattering*, Academic Press, New York (1967).
- [7] P. Roman, *Advanced Quantum Theory: An Outline of the Fundamental Ideas*, Addison-Wesley, Reading, Massachusetts (1965).
- [8] K. M. Jones, and E. Tiesinga, P.D. Lett, and P. S. Julienne, *Rev. Mod. Phys.*, **78**, 483 (2006).
- [9] E. R. I. Abraham, W. I. McAlexander, C. A. Sackett, and R. G. Hullet, *Phys. Rev. Lett.*, **74**, 1315 (1995).
- [10] O. Dulieu and P.S. Julienne, *J. Chem. Phys.*, **103**, 60 (1995).
- [11] G. Gutiérrez, M. de Llano, and W. C. Stwalley, *Phys. Rev. B*, **29**, 5211 (1984).
- [12] M. Marinescu, *Phys. Rev. A*, **50**, 3177 (1994).
- [13] R. Szmjtkowski, *J. Phys. A: Math. Gen.*, **28**, 7333 (1995).
- [14] H. Ouerdane, M. J. Jamieson, D. Vrinceanu and M. J. Cavagnero, *J. Phys. B: At. Mol. Opt. Phys.*, **36**, 4055 (2003).
- [15] G. F. Gribakin and V. V. Flambaum, *Phys. Rev. A*, **48**, 546 (1993).
- [16] M.S. Child, *Semiclassical Mechanics with Molecular Applications*, Clarendon Press, Oxford (1991).
- [17] J. Liouville, *J. Math. Pure Appl.*, **2**, 16 (1837); G. Green, *Trans. Cambridge Phil. Soc.*, **6**, 457 (1837).
- [18] V. V. Meshkov, A. V. Stolyarov, and R. J. Le Roy, *Phys. Rev. A*, **78**, 052510 (2008).
- [19] J. F. Ogilvie, *Proc. Roy. Soc. (London) A*, **378**, 287 (1981).
- [20] A. A. Surkus, R. J. Rakauskas, and A. B. Bolotin, *Chem. Phys. Lett.*, **105**, 291 (1984).
- [21] B. Numerov, *Publ. Obs. Cent. Astrophys. Russ.*, **2**, 188 (1933).
- [22] J. P. Boyd, *Chebyshev and Fourier Spectral Methods*, DOVER Publications, Inc., New York (2000).
- [23] B.R. Johnson, *J. Comp. Phys.*, **13**, 445 (1973).
- [24] B.R. Johnson, *J. Chem. Phys.*, **67**, 4086 (1977).
- [25] L. F. Richardson, *Phil. Trans. Roy. Soc. (London) A*, **226**, 299 (1927).
- [26] W. H. Press, S. A. Teukolsky, W. T. Vetterling, and B. P. Flannery, *Numerical Recipes in Fortran 77*, Cambridge University Press (1999).
- [27] E. Czuchaj, J. Sienkiewicz and W. Miklaszewski, *Chem. Phys.*, **116**, 69 (1987).
- [28] R. A. Aziz, V. P. S. Nain, J. S. Carley, W. L. Taylor and G. T. McConville, *J. Chem. Phys.*, **70**, 4330 (1979).
- [29] A FORTRAN 77 code for performing the *s*-wave scattering length calculation based on the adaptive mapping procedure has been deposited in the journal's on-line electronic archive. E-PAPS document files can be retrieved via the EPAPS homepage (<http://www.aip.org/epaps/epaps.html>) or from <ftp.aip.org> in the directory/epaps/. See the EPAPS homepage for more information.
- [30] R. J. Le Roy, *A Computer Program for Solving the Radial Schrödinger Equation for Bound and Quasibound Levels and Scattering Lengths*, University of Waterloo Chemical Physics Research Report CP-XXX (2011); see <http://leroy.uwaterloo.ca/programs/>.